

Pattern formations of 2D Rayleigh–Bénard convection with no-slip boundary conditions for the velocity at the critical length scales

Taylan Sengul^a, Jie Shen^b and Shouhong Wang^{c*†}

Communicated by R. Showalter

We study the Rayleigh–Bénard convection in a 2D rectangular domain with no-slip boundary conditions for the velocity. The main mathematical challenge is due to the no-slip boundary conditions, because the separation of variables for the linear eigenvalue problem, which works in the free-slip case, is no longer possible. It is well known that as the Rayleigh number crosses a critical threshold R_c , the system bifurcates to an attractor, which is an $(m-1)$ -dimensional sphere, where m is the number of eigenvalues, which cross zero as R crosses R_c . The main objective of this article is to derive a full classification of the structure of this bifurcated attractor when $m = 2$. More precisely, we rigorously prove that when $m = 2$, the bifurcated attractor is homeomorphic to a one-dimensional circle consisting of exactly four or eight steady states and their connecting heteroclinic orbits. In addition, we show that the mixed modes can be stable steady states for small Prandtl numbers. Copyright © 2014 John Wiley & Sons, Ltd.

Keywords: Bénard convection; dynamic transition; pattern formation

1. Introduction

The Rayleigh–Bénard convection problem is one of the fundamental problems in the physics of fluids. The basic phenomena of the Rayleigh–Bénard convection in horizontally extended systems are widely known. The influence of the side walls, although not studied as thoroughly as the horizontally extended case, is of practical importance for engineering applications.

In this paper, we study the Rayleigh–Bénard convection in a 2D rectangular domain with no-slip boundary conditions for the velocity. This problem is also closely related to the problem of infinite channel with rectangular cross section, which has been studied by Davies-Jones [1], Luijckx and Platten [2], and Kato and Fujimura [3], among others.

The linear aspects of the problem we consider in this paper have been studied by Lee *et al.* [4], Mizushima [5], and Gelfgat [6]. In these papers, the critical Rayleigh number and the structure of the critical eigenmodes have been studied for small aspect ratio containers.

From dynamical transition and pattern formation point of view, Ma and Wang [7,8] proved that under some general boundary conditions, the problem always undergoes a dynamic transition to an attractor Σ_R as the Rayleigh number R crosses the first critical Rayleigh number R_c . They also proved that the bifurcated attractor is homological to S^{m-1} , where m is the number of critical eigenmodes.

In the 2D setting that we consider, m is either 1 or 2, and the latter case can only happen at the critical length scales where two modes with wave numbers k and $k+1$ become critical simultaneously. When $m = 1$, the structure of Σ_R is trivial, which is merely a disjoint union of two attracting steady states. Thus, our task in this paper is to classify the structure of the attractor when $m = 2$. This has been studied recently in [9] for the 3D Rayleigh–Bénard problem where the boundaries were assumed to be free slip for the velocity and the wave numbers of the critical modes were assumed to be equal.

The main mathematical challenge in this paper is due to the no-slip boundary conditions because the separation of variables for the linear eigenvalue problem, which works in the free-slip case, is not possible anymore. To overcome this difficulty, the main approach for our study is to combine rigorous analysis and numerical computation using spectral method.

^a Department of Mathematics, Yeditepe University, 34750 Istanbul, Turkey

^b Department of Mathematics, Purdue University, West Lafayette, IN, USA

^c Department of Mathematics, Indiana University, Bloomington, IN, USA

* Correspondence to: Shouhong Wang, Department of Mathematics, Indiana University, Bloomington, IN, USA.

† E-mail: showang@indiana.edu

As we know, spectral methods have long been used to address the hydrodynamic instability problems. In fact, in his seminal work [10], Orszag studied the classical Orr–Sommerfeld linear instability problem using a Chebyshev-tau method. In this paper, to treat the linear eigenvalue problem, we employ a Legendre–Galerkin method where compact combinations of Legendre polynomials, also called generalized Jacobi polynomials, satisfying all the boundary conditions are used as trial functions. The main advantage of Legendre–Galerkin method is that the resulting matrices are sparse, which allows a very efficient and accurate solution of the linearized problem; see also Hill and Straughan [11] and Gheorghiu and Dragomirescu [12].

Once the eigenpairs of the linear problem are identified, the transition analysis is carried out by reducing the infinite dimensional system to the center manifold in the first two critical eigendirections. The coefficients of this reduced system are calculated numerically. Our main results are described later.

We first classify the eigenmodes into four classes according to their parities using the symmetry of the problem. Then, we numerically show that the first two unstable modes are always parity class 1 or 2. Then, we study the transition near the critical length scales where two eigenvalues become positive simultaneously. Next, we rigorously prove that the local attractor at small supercritical Rayleigh numbers is in fact homeomorphic to the circle, which has four or eight steady states with half of them as stable points and the rest as saddle points. The critical eigenmodes are always bifurcated steady states on the attractor, and when the attractor has eight steady states, the mixed modes, which are superpositions of the critical eigenmodes, are also bifurcated.

Second, let β_1 and β_2 denote the two largest eigenvalues of the linearized problem. We find that a small neighborhood of $\beta_1 = \beta_2 = 0$ in the β_1 – β_2 plane can be separated into several sectors with different asymptotical structures. In particular, we find that there is a critical Prandtl number Pr_c for the first two critical length scales $L = 1.5702$ and $L = 2.6611$, such that for $Pr < Pr_c$, there is a sector in this plane for which mixed modes are stable fixed points of the attractor. For $Pr > Pr_c$, the mixed modes are never stable, and instead, there is a sector in this plane in which both of the critical eigenmodes coexist as stable steady states. In this case, the initial conditions determine which one of these eigenmodes will be realized. The critical Prandtl number Pr_c is around 0.14 for the first critical length scale $L = 1.5702$ and around 0.05 for the second critical length scale $L = 2.6611$. For higher critical length scales, we found that mixed modes are never stable points of the attractor.

Third, recently, Ma and Wang have developed the dynamic transition theory to study transition and bifurcation problems in nonlinear sciences; see [13]. This paper is a first attempt to combine this theory with the numerical tools of the spectral methods to study the detailed structure of the transition and pattern formation.

The paper is organized as follows. In Section 2, the governing equations and the functional setting of the problem are discussed. In Section 3, linear eigenvalue problem is studied. Section 4 states the main theorem. Section 5 is devoted to the proof of the main theorem. In Section 6, we demonstrate a method to compute the coefficients of the reduced system. And the last section discusses the results obtained by our analysis.

2. Governing equations and the functional setting

Two-dimensional thermal convection with no-slip, perfectly conducting boundaries can be modeled by the Boussinesq equations. The governing equations on the rectangular domain $\Omega = (0, L) \times (0, 1) \in \mathbb{R}^2$ read as

$$\begin{aligned} \frac{\partial \mathbf{u}}{\partial t} + (\mathbf{u} \cdot \nabla) \mathbf{u} &= Pr(-\nabla p + \Delta \mathbf{u}) + \sqrt{R} \sqrt{Pr} \theta \mathbf{k}, \\ \frac{\partial \theta}{\partial t} + (\mathbf{u} \cdot \nabla) \theta &= \sqrt{R} \sqrt{Pr} w + \Delta \theta, \\ \nabla \cdot \mathbf{u} &= 0. \end{aligned} \quad (1)$$

Here, $\mathbf{u} = (u, w)$ is the velocity field, θ is the temperature field, and p is the pressure field. These fields represent a perturbation around the motionless state with a linear temperature profile. The dimensionless numbers are the Prandtl number Pr and the Rayleigh number R , which is also the control parameter. \mathbf{k} represents the unit vector in the z -direction.

The equations (1) are supplemented with no-slip boundary conditions for the velocity and perfectly conducting boundary conditions for the temperature.

$$\mathbf{u} = \theta = 0, \quad \text{on } \partial\Omega. \quad (2)$$

For the functional setting, we define the relevant function spaces:

$$\begin{aligned} H &= \{(\mathbf{u}, \theta) \in L^2(\Omega, \mathbb{R}^3) : \nabla \cdot \mathbf{u} = 0, \mathbf{u} \cdot \mathbf{n} |_{\partial\Omega} = 0\}, \\ H_1 &= \{(\mathbf{u}, \theta) \in H^2(\Omega, \mathbb{R}^3) : \nabla \cdot \mathbf{u} = 0, \mathbf{u} |_{\partial\Omega} = 0, \theta |_{\partial\Omega} = 0\}. \end{aligned} \quad (3)$$

For $\phi = (\mathbf{u}, \theta)$, let $G : H_1 \rightarrow H$ and $L_R : H_1 \rightarrow H$ be defined by

$$\begin{aligned} L_R \phi &= (\mathcal{P}(Pr \Delta \mathbf{u} + \sqrt{R} \sqrt{Pr} \theta \mathbf{k}), \sqrt{R} \sqrt{Pr} w + \Delta \theta), \\ G(\phi) &= -(\mathcal{P}(\mathbf{u} \cdot \nabla) \mathbf{u}, (\mathbf{u} \cdot \nabla) \theta), \end{aligned} \quad (4)$$

with \mathcal{P} denoting the Leray projection onto the divergence-free vectors.

The equations (1)–(2) supplemented with initial conditions can be put into the following abstract ordinary differential equation:

$$\frac{d\phi}{dt} = L_R\phi + G(\phi), \quad \phi(0) = \phi_0. \tag{5}$$

For results concerning the existence and uniqueness of solutions of (5), we refer to Foias *et al.* [14]. Finally, for $\phi_i = (\mathbf{u}_i, \theta_i)$, $\mathbf{u}_i = (u_i, w_i)$, $i = 1, 2, 3$, we define the following trilinear forms.

$$\begin{aligned} G(\phi_1, \phi_2, \phi_3) &= - \int_{\Omega} (\mathbf{u}_1 \cdot \nabla) \mathbf{u}_2 \cdot \mathbf{u}_3 \, dx dz - \int_{\Omega} (\mathbf{u}_1 \cdot \nabla) \theta_2 \cdot \theta_3 \, dx dz, \\ G_s(\phi_1, \phi_2, \phi_3) &= G(\phi_1, \phi_2, \phi_3) + G(\phi_2, \phi_1, \phi_3). \end{aligned} \tag{6}$$

3. Linear analysis

We first study the eigenvalue problem $L_R\phi = \beta\phi$, which reads as

$$\begin{aligned} \Pr \left(\Delta u - \frac{\partial p}{\partial x} \right) &= \beta u, \\ \Pr \left(\Delta w - \frac{\partial p}{\partial z} \right) + \sqrt{R} \sqrt{\Pr} \theta &= \beta w, \\ \Delta \theta + \sqrt{R} \sqrt{\Pr} w &= \beta \theta, \\ \operatorname{div} \mathbf{u} &= 0, \\ u = \theta &= 0, \quad \text{at } \partial\Omega. \end{aligned} \tag{7}$$

In the following, we list some of the properties of this eigenvalue problem.

1. The linear operator L_R is symmetric. Hence, the eigenvalues β_i are real, and the eigenfunctions ϕ_i are orthogonal with respect to L^2 -inner product. Moreover, there is a sequence

$$0 < R_1 \leq R_2 \leq \dots$$

such that $\beta_i(R_i) = 0$. R_i is found by setting $\beta = 0$ in (7). In this case, the problem becomes an eigenvalue problem with \sqrt{R} as the eigenvalue.

2. We have

$$\beta_i(R) \begin{cases} \geq 0 & \text{if } R \geq R_i, \\ < 0 & \text{if } R < R_i, \end{cases}$$

which can be seen by computing the derivative of β_i with respect to R at $R = R_i$.

$$\frac{d\beta_i}{dR} \Big|_{R=R_i} = \frac{1}{\sqrt{R_i}} \frac{\int_{\Omega} \theta_i w_i \, dx dz}{\int_{\Omega} (u_i^2 + w_i^2 + \theta_i^2) \, dx dz}, \tag{8}$$

where (u_i, w_i, θ_i) is the i^{th} eigenfunction. Also at $R = R_i$, by the third equation in (7), $w_i = -R_i^{-1/2} \Pr^{-1/2} \Delta \theta_i$ as $\beta_i(R_i) = 0$. Plugging these into (8) and integrating by parts, we see that

$$\frac{d\beta_i}{dR} \Big|_{R=R_i} = \frac{\int_{\Omega} |\nabla \theta_i|^2 \, dx dz}{R_i \int_{\Omega} (|u_i|^2 + |w_i|^2 + |\theta_i|^2) \, dx dz} > 0.$$

3. We denote the critical Rayleigh number $R_c = R_1$. That is,

$$\begin{aligned} \beta_i(R) &\begin{cases} < 0 & \text{if } R < R_c, \\ = 0 & \text{if } R = R_c, \\ > 0 & \text{if } R > R_c. \end{cases} \quad i = 1, \dots, m \\ \beta_i(R_c) &< 0, \quad i > m. \end{aligned} \tag{9}$$

m in (9) does not depend on the Prandtl number \Pr but only on L . To see this, one makes the change of variable $\theta = \sqrt{\Pr} \theta'$ so that the solution of (7) for the eigenvalue of $\beta = 0$ is independent of \Pr . By simplicity of the first eigenvalue (see Theorem 3.7 in the study of Ma and Wang [15]), for almost every value of L except a discrete set of values, m in (9) is 1.

Table I. Possible parity classes of the eigenfunctions of the linear operator.			
Class 1	Class 2	Class 3	Class 4
$\psi(e, e), \theta(o, e)$	$\psi(o, e), \theta(e, e)$	$\psi(e, o), \theta(o, o)$	$\psi(o, o), \theta(e, o)$

Introducing the stream function $\psi_z = u, \psi_x = -w$, we can eliminate the pressure p from the linear eigenvalue problem (7).

$$\begin{aligned} \text{Pr} \Delta^2 \psi - \sqrt{R} \sqrt{\text{Pr}} \theta_x &= \beta(R) \Delta \psi, \\ -\sqrt{R} \sqrt{\text{Pr}} \psi_x + \Delta \theta &= \beta(R) \theta, \\ \psi = \frac{\partial \psi}{\partial n} = \theta &= 0 \text{ on } \partial \Omega. \end{aligned} \tag{10}$$

The linear equations (7) satisfy several discrete symmetries, which may be found from the known non-trivial groups of continuous Lie symmetries of the field equations (1); see Hydon [16] and Marques *et al.* [17]. However, for the problem we consider, it can be easily verified that the linear equations have reflection symmetries about the horizontal and vertical mid-planes of the domain. Thus, we can classify the solutions of the linear problem into four classes with different parities as defined in Table I where, for example, $\psi(o, e)$ means that ψ is odd in the x -direction and even in the z -direction.

We will employ a Legendre–Galerkin method (cf. Shen [18]; Shen *et al.* [19]) to solve the linear eigenvalue problem (10). For this, first, we transform the domain with the change of variable

$$(x, z) \in (0, L) \times (0, 1) \rightarrow (x', z') = \left(\frac{2x}{L} - 1, 2z - 1 \right) \in (-1, 1)^2.$$

For notational simplicity, we will omit the primes and write $(x, z) \in (-1, 1)^2$. The approximate solutions (ψ^N, θ^N) of (10) will be sought in the finite dimensional space, which is the span of

$$\{ (e_j(x) e_k(z), f_l(x) f_m(z)) \mid j, l = 0, \dots, N_x - 1, k, m = 0, \dots, N_z - 1 \},$$

where e_j and f_j are generalized Jacobi polynomials (cf. Guo *et al.* [20]; Shen *et al.* [19]), which satisfy the boundary conditions

$$e_i(\pm 1) = D e_i(\pm 1) = f_i(\pm 1) = 0.$$

Here, D denotes the derivative. The polynomials e_i and f_i are defined as in chapter 6 of Shen *et al.* [19],

$$f_i(z) = L_i(z) - L_{i+2}(z), \tag{11}$$

$$e_i(z) = \frac{L_i(z) - \frac{4i+10}{2i+7} L_{i+2}(z) + \frac{2i+3}{2i+7} L_{i+4}(z)}{(2i+3)(4i+10)^{1/2}}, \tag{12}$$

where L_i is the i^{th} Legendre polynomial. The coefficient of e_i guarantees that $(D^2 e_i, D^2 e_j) = \delta_{ij}$.

We write the approximate solutions of equation (10) with coefficients to be determined by

$$\psi^N = \sum_{j=0}^{N_x-1} \sum_{k=0}^{N_z-1} \tilde{\psi}_{jk}^N e_j(x) e_k(z), \quad \theta^N = \sum_{j=0}^{N_x-1} \sum_{k=0}^{N_z-1} \tilde{\theta}_{jk}^N f_j(x) f_k(z). \tag{13}$$

Here, $N = 2N_x N_z$ denotes the total degrees of freedom.

Let us define for $i, j = 0, \dots, m - 1$,

$$\begin{aligned} (A_1^m)_{ij} &= (D^2 e_i, D^2 e_j) = \delta_{ij}, & (A_2^m)_{ij} &= (D^2 e_i, e_j) = -(D e_j, D e_i), \\ (A_3^m)_{ij} &= (e_i, e_j), & (A_4^m)_{ij} &= (e_i, f_j), \\ (A_5^m)_{ij} &= (D^2 f_i, f_j), & (A_6^m)_{ij} &= (f_i, f_j), \\ (A_7^m)_{ij} &= (D f_i, e_j), \end{aligned}$$

and for $j = 0, \dots, N_x - 1, k = 0, \dots, N_z - 1$,

$$\tilde{\psi}^N = \{ \tilde{\psi}_{jk}^N \}, \quad \tilde{\theta}^N = \{ \tilde{\theta}_{jk}^N \}.$$

By using the following property of the Legendre polynomials

$$(2i + 3)L_{i+1} = D(L_{i+2} - L_i), \tag{14}$$

it is easy to see that

$$De_i(z) = \frac{L_{i+3} - L_{i+1}}{\sqrt{4i + 10}}, D^2e_i(z) = \sqrt{\frac{2i + 5}{2}}L_{i+2}(z), Df_i = -(2i + 3)L_{i+1}. \tag{15}$$

By (15), it is easy to determine the elements of the matrices A_k by the orthogonality of the Legendre polynomials. In particular, the matrices A_1^m, \dots, A_7^m are banded, and except for A_4^m and A_7^m , they are symmetric.

Putting (13) into (10), multiplying the resulting equations by $e_m(x)e_n(z)$ and $f_m(x)f_n(z)$, respectively, and integrating over $-1 \leq x \leq 1$, $-1 \leq z \leq 1$ to obtain

$$B^N \bar{x}^N - \sqrt{RC}^N \bar{x}^N = \beta^N(R)D^N \bar{x}^N. \tag{16}$$

Here,

$$\begin{aligned} B^N &= \begin{bmatrix} \text{Pr} X_1 & 0 \\ 0 & X_3 \end{bmatrix}_{N \times N}, & C^N &= \begin{bmatrix} 0 & \sqrt{\text{Pr}} X_2 \\ -\sqrt{\text{Pr}} X_2^T & 0 \end{bmatrix}_{N \times N}, \\ D^N &= \begin{bmatrix} X_4 & 0 \\ 0 & X_5 \end{bmatrix}_{N \times N}, & \bar{x}^N &= \begin{bmatrix} \text{vec}(\tilde{\psi}^N) \\ \text{vec}(\tilde{\theta}^N) \end{bmatrix}_{N \times 1}, \end{aligned} \tag{17}$$

where

$$\begin{aligned} X_1 &= \frac{2^4}{L^4} A_3^{N_z} \otimes A_1^{N_x} + \frac{2^5}{L^2} A_2^{N_z} \otimes A_2^{N_x} + 2^4 A_1^{N_z} \otimes A_3^{N_x}, \\ X_2 &= \frac{2}{L} A_4^{N_z} \otimes (A_7^{N_x})^T, & X_3 &= \frac{2^2}{L^2} A_6^{N_z} \otimes A_5^{N_x} + 2^2 A_5^{N_z} \otimes A_6^{N_x}, \\ X_4 &= \frac{2^2}{L^2} A_3^{N_z} \otimes A_2^{N_x} + 2^2 A_2^{N_z} \otimes A_3^{N_x}, & X_5 &= A_6^{N_z} \otimes A_6^{N_x}. \end{aligned} \tag{18}$$

In (17) and (18), we use the following notations. For an $m \times k$ matrix M , $\text{vec}(M)$ is the $mk \times 1$ column vector obtained by concatenating the columns M_j of M , that is,

$$\text{vec}([M_1 \ M_2 \ \dots \ M_k]) = [M_1^T \ M_2^T \ \dots \ M_k^T]^T.$$

0 stands for the zero matrix. If A is an $m \times n$ matrix and B is $p \times q$, then $A \otimes B = \{a_{ij}B\}$, the Kronecker product of A and B , is an $mp \times nq$ matrix defined as

$$A \otimes B = \begin{bmatrix} a_{11}B & \dots & a_{1n}B \\ \vdots & \ddots & \vdots \\ a_{m1}B & \dots & a_{mn}B \end{bmatrix}.$$

To obtain (16), we used the following properties of the Kronecker product.

- If A, B , and X are three matrices such that AXB is defined, then

$$\text{vec}(AXB) = (B^T \otimes A)\text{vec}(X).$$

- $(A \otimes B)^T = A^T \otimes B^T$.

We note that the matrices B^N, C^N , and D^N in (16) are sparse, B^N and D^N are symmetric, and C^N is skew-symmetric. From our linear analysis, we find the following results.

- Our numerical analysis suggest that $N_x = 6 + 2k \approx 6 + 2L$ and $N_z = 8$ is enough to resolve the critical Rayleigh number and the first critical mode, which has k rolls in its stream function. We have checked that increasing N_x and N_z by two only modifies the fourth or fifth significant digit of the result.
- In Figure 1, the first critical mode is shown for the length scales $L = 1, \dots, 4$. Note that the first critical stream function and the temperature distribution have always even parity in the z -direction while their x -parity alternates between odd and even as the length scale increases. As observed by Mizushima [5], we also verify the existence of the Moffatt vortices on the corners of the domain, which are due to corner singularities as shown in Figure 2.
- For $L < 21$, we observed that m in (9) is either 1 or 2. Moreover, $m = 2$ only at the critical length scales, which are given in Table II. The results found are in agreement with those in the study of Mizushima [5] and Lee *et al.* [4].
- The marginal stability curves of the first few critical eigenvalues are given in Figure 3. The figure demonstrates that the parities of the first two critical modes can only be of parity class 1 or 2 as given in Table I.

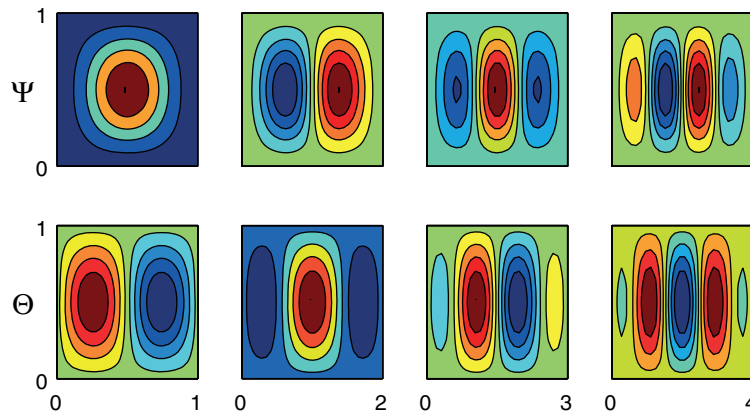


Figure 1. ψ (on top) and θ (on bottom) of the first critical mode for $L = 1, \dots, 4$.

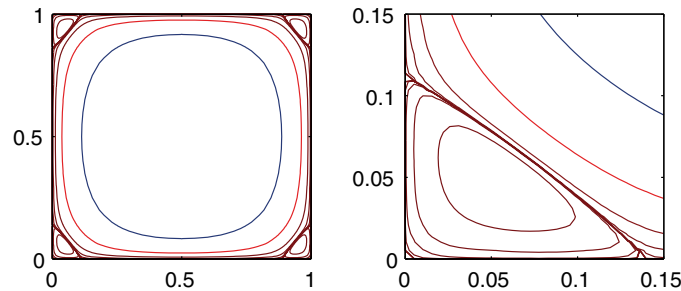


Figure 2. The left figure shows the plot of the first critical stream function for $L = 1$ (the top left plot in Figure 1). The right figure shows the corner details of the left figure.

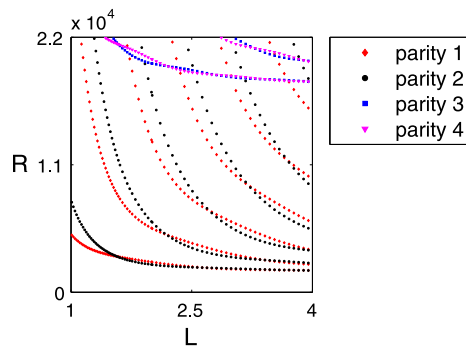


Figure 3. The marginal stability curves of the first few eigenvalues with eigenfunctions of different parity classes.

Also it is seen in these figures that there is a repulsion of the eigenvalues. Namely, the neutral stability curves of the same parity type do not intersect each other. Such a repulsion does not occur for free-slip boundary conditions. This repulsion arises from a structural instability of the transform of matrices into a Jordan canonical form, and a detailed analysis can be found in the study of Mizushima and Nakamura [21].

4. Main theorem

Let m be the number of modes, which become critical as the first Rayleigh number R_c is crossed as given by (9). Ma and Wang [7, 8] proved that under some general boundary conditions, the problem has an attractor Σ_{R_c} , which bifurcates from $(0, R_c)$ as R crosses R_c . They also proved that the dimension of the bifurcated attractor is $m - 1 \leq \dim(\Sigma_R) \leq m$. When $m = 1$, the structure of Σ_R is trivial, which is merely a disjoint union of two attracting steady states.

As stated before, in our problem, m is either 1 or 2. And the latter case can only happen at a critical length scale L_c where two eigenmodes with consecutive wave numbers become critical.

Numerically, it turns out that the critical Rayleigh numbers for modes with parity 3 or 4 are much greater than those for modes with parity 1 or 2. This can be seen from Figure 3.

Table II. At $L = L_c$, two modes become unstable.							
L_c	k	R_c	N_x	L_c	k	R_c	N_x
1.5702	1	3086.6554	8	6.7711	6	1764.3754	18
2.6611	2	2113.776	10	8.7992	8	1740.9174	22
3.7048	3	1906.3395	12	10.8229	10	1729.5398	26
4.7329	4	1826.4099	14	15.8738	15	1717.805	36
5.7541	5	1786.8833	16	20.9197	20	1713.5226	46

One of the modes has k , and the other one has $k + 1$ rolls in x -direction in their stream functions. The critical Rayleigh number at this length scale is R_c . N_x and N_z are the number of polynomials used in the x and z directions, respectively, with $N_z = 8$ fixed.

We will assume the following.

1. $(\beta_1, \phi_1), (\beta_2, \phi_2)$ are the first two critical eigenpairs.
2. ϕ_1 has wave number k , ϕ_2 has wave number $k + 1$ where k is a positive integer.
3. One of the eigenmodes $\{\phi_1, \phi_2\}$ is of parity class 1, while the other is of parity class 2 as given in Table I.

Consider a solution ϕ of (5)

$$\phi = \sum_{i=1}^{\infty} y_i \phi_i$$

with sufficiently small initial data. Then, in the proof of the main theorem, we show that the dynamics of the system close to $R = R_c$ and $L = L_c$ is governed by the equations

$$\begin{aligned} \frac{dy_1}{dt} &= \beta_1 y_1 + y_1 (a_{11} y_1^2 + a_{13} y_2^2) + o(3), \\ \frac{dy_2}{dt} &= \beta_2 y_2 + y_2 (a_{22} y_1^2 + a_{24} y_2^2) + o(3). \end{aligned} \tag{20}$$

Here, β_i is the eigenvalue corresponding to mode i , and $o(3)$ denotes

$$o(3) = o(|(y_1, y_2)|^3) + O\left(|(y_1, y_2)|^3 \max_{i=1,2} |\beta(R)|\right).$$

Let us define

$$D_1 = a_{22}\beta_1 - a_{11}\beta_2, \quad D_2 = a_{13}\beta_2 - a_{24}\beta_1, \quad D_3 = a_{11}a_{24} - a_{13}a_{22}. \tag{21}$$

To state our main theorems, we assume the following non-degeneracy conditions

$$a_{11} \neq 0, a_{24} \neq 0, D_1 \neq 0, D_2 \neq 0, D_3 \neq 0. \tag{22}$$

Finally, let us define the following.

$$\begin{aligned} \varphi_i &= (-1)^i \phi_1, & i &= 1, 2, \\ \varphi_i &= (-1)^i \phi_2, & i &= 3, 4, \\ \varphi_i &= c_i \phi_1 + d_i \phi_2, & i &= 5, 6, 7, 8, \end{aligned} \tag{23}$$

where $c_5 = c_6 = -c_7 = -c_8$ and $d_5 = -d_6 = d_7 = -d_8$.

Thus, φ_1 and φ_2 are modes with wave number k , φ_3 and φ_4 are modes with wave number $k + 1$, and $\varphi_5, \dots, \varphi_8$ are mixed modes meaning that they are superpositions of the modes with wave numbers k and $k + 1$.

Theorem 4.1

Under the assumptions (19) and (22), there is an attractor Σ_R bifurcating as R crosses R_c , which is homeomorphic to the circle S^1 when L is sufficiently close to a critical length scale L_c . Moreover, Σ_R consists of steady states and their connecting heteroclinic orbits. Let $n(\Sigma_R)$ denote the number of steady states on Σ_R , \mathcal{S} denote the stable steady states, and \mathcal{U} denote the unstable steady states on Σ_R up to topological equivalency. Then, we have the following characterization of Σ_R , which is also illustrated in Figure 4.

- (i) If $D_1 < 0, D_2 < 0, D_3 < 0, n(\Sigma_R) = 8, \mathcal{S} = \{\varphi_i \mid i = 1, 2, 3, 4\}, \mathcal{U} = \{\varphi_i \mid i = 5, 6, 7, 8\}$.
- (ii) If $D_1 > 0, D_2 > 0, D_3 > 0, n(\Sigma_R) = 8, \mathcal{S} = \{\varphi_i \mid i = 5, 6, 7, 8\}, \mathcal{U} = \{\varphi_i \mid i = 1, 2, 3, 4\}$.
- (iii) If $D_1 < 0, D_2 > 0, n(\Sigma_R) = 4, \mathcal{S} = \{\varphi_i \mid i = 1, 2\}, \mathcal{U} = \{\varphi_i \mid i = 3, 4\}$.
- (iv) If $D_1 > 0, D_2 < 0, n(\Sigma_R) = 4, \mathcal{S} = \{\varphi_i \mid i = 3, 4\}, \mathcal{U} = \{\varphi_i \mid i = 1, 2\}$.

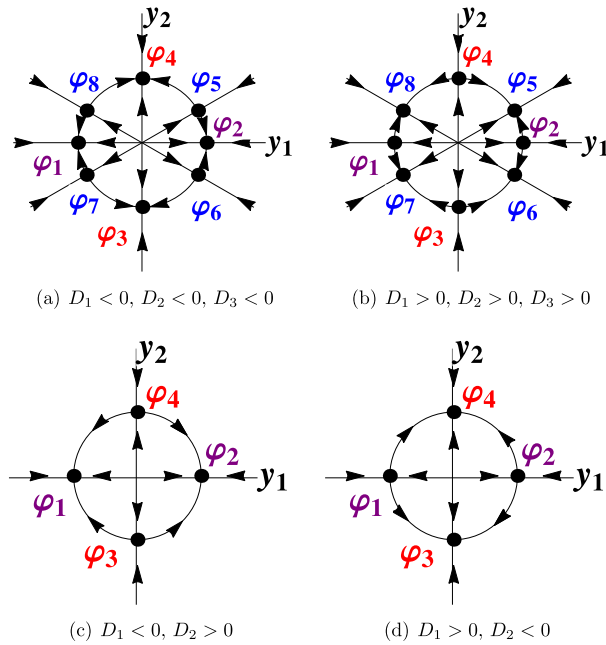


Figure 4. Transition scenarios.

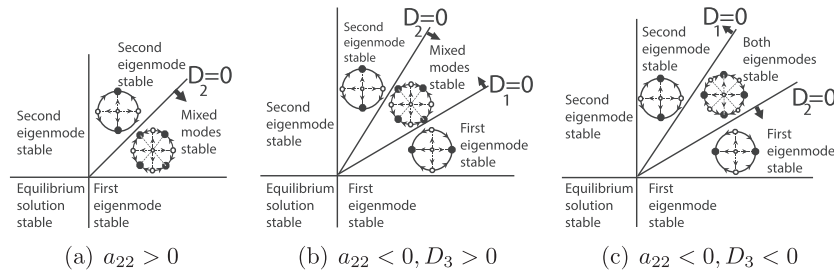


Figure 5. The transition scenarios in β_1 - β_2 plane. In the previous cases, we assume that $a_{13} < 0$, which is due to our numerical observations. The arrows on the lines $D_1 = 0, D_2 = 0$ indicate in which directions D_1 and D_2 increase. First and second eigenmodes correspond to the eigenmodes with wave number k and $k + 1$, respectively.

According to Theorem 4.1, the structure of the attractor depends on D_1, D_2 , and D_3 , which in turn depends on the coefficients of the reduced equations. By (21), D_3 has a definite sign whereas D_1 and D_2 vanish at the criticality $\beta_1 = \beta_2 = 0$. In the proof of Theorem 4.1, we analytically prove that the coefficients a_{11} and a_{24} are negative. Our numerical computations indicate that a_{13} is also always negative. We observed that a_{22} and D_3 can be both positive and negative.

That gives three possible cases depending on the signs of a_{22} and D_3 . In Figure 5, we classify these cases in a small neighborhood of $\beta_1 = \beta_2 = 0$ in the β_1 - β_2 plane according to our main theorem and the following observations.

- If $a_{22} > 0$, then $D_3 > 0, D_1 > 0$, but D_2 changes sign in the first quadrant.
- If $a_{22} < 0$ and $D_3 > 0$, then D_1 and D_2 change sign in the first quadrant. Moreover, the case where both $D_1 < 0$ and $D_2 < 0$ is not possible.
- If $a_{22} < 0$ and $D_3 < 0$, then again D_1 and D_2 change sign in the first quadrant. This time the case where both $D_1 > 0$ and $D_2 > 0$ is not possible.

5. Proof of the main theorem

We will give the proof in several steps.

Step 1. The reduced equations. When there are two critical modes ϕ_1, ϕ_2 , the center manifold is a 2D manifold embedded in the infinite dimensional space. We denote the center manifold function by

$$\Phi = y_1^2 \Phi_1 + y_1 y_2 \Phi_2 + y_2^2 \Phi_3 + o(y^2), \quad \Phi_i = (U_i, W_i, \Theta_i).$$

To study the dynamics on the center manifold, we plug in

$$\phi = y_1\phi_1 + y_2\phi_2 + y_1^2\Phi_1 + y_1y_2\Phi_2 + y_2^2\Phi_3 + o(2), \quad (24)$$

into (5), take the inner product with ϕ_1, ϕ_2 , and use the orthogonality of the eigenvectors, thanks to the self-adjointness of the linear operator. The reduced equations read

$$\frac{dy_i}{dt} = \beta_i(R)y_i + \frac{1}{(\phi_i, \phi_i)}(G(\phi), \phi_i), \quad i = 1, 2 \quad (25)$$

We normalize the first two eigenfunctions so that

$$(\phi_1, \phi_1) = (\phi_2, \phi_2) = 1.$$

Now if we expand the nonlinear terms in (25), we obtain

$$\begin{aligned} \frac{dy_1}{dt} &= \beta_1 y_1 + (a_{11}y_1^3 + a_{12}y_1^2y_2 + a_{13}y_1y_2^2 + a_{14}y_2^3) + o(3), \\ \frac{dy_2}{dt} &= \beta_2 y_2 + (a_{21}y_1^3 + a_{22}y_1^2y_2 + a_{23}y_1y_2^2 + a_{24}y_2^3) + o(3), \end{aligned} \quad (26)$$

where

$$\begin{aligned} a_{k1} &= G_5(\phi_1, \Phi_1, \phi_k), & a_{k2} &= G_5(\phi_1, \Phi_2, \phi_k) + G_5(\phi_2, \Phi_1, \phi_k), \\ a_{k4} &= G_5(\phi_2, \Phi_3, \phi_k), & a_{k3} &= G_5(\phi_1, \Phi_3, \phi_k) + G_5(\phi_2, \Phi_2, \phi_k). \end{aligned} \quad (27)$$

Step 2. Parities of the center manifold functions. To compute the center manifold approximation, we will use the following formula, which was introduced by Ma and Wang [15].

$$\begin{aligned} -\mathcal{L}_R\Phi_1 &= P_2G(\phi_1, \phi_1), \\ -\mathcal{L}_R\Phi_2 &= P_2[G(\phi_1, \phi_2) + G(\phi_2, \phi_1)], \\ -\mathcal{L}_R\Phi_3 &= P_2G(\phi_2, \phi_2). \end{aligned} \quad (28)$$

Here,

$$\begin{aligned} P_2 : H &\rightarrow E_2, & \mathcal{L}_R &= L_R|_{E_2} : E_2 \rightarrow \bar{E}_2, \\ E_1 &= \text{span}\{\phi_1, \phi_2\}, & E_2 &= E_1^\perp. \end{aligned}$$

Let $\mathcal{X} = \{f \in C(\Omega) \mid f(-x, z) = \pm f(x, z) \text{ and } f(x, -z) = \pm f(x, z)\}$, and let $s : \mathcal{X} \rightarrow \{\pm 1\}^2$ denote the parity function:

$$s(f) = (s_x(f), s_z(f)),$$

where

$$s_x(f) = \pm 1 \quad \text{if } f(-x, z) = \pm f(x, z), \quad s_z(f) = \pm 1 \quad \text{if } f(x, -z) = \pm f(x, z).$$

Let us define for $\phi_i = (u_i, w_i, \theta_i), i = 1, 2$, the following.

$$G(\phi_i, \phi_j) = \begin{bmatrix} g_1(\phi_i, \phi_j) \\ g_2(\phi_i, \phi_j) \\ g_3(\phi_i, \phi_j) \end{bmatrix} = \begin{bmatrix} -u_i \frac{\partial u_j}{\partial x} - w_i \frac{\partial u_j}{\partial z} \\ -u_i \frac{\partial w_j}{\partial x} - w_i \frac{\partial w_j}{\partial z} \\ -u_i \frac{\partial \theta_j}{\partial x} - w_i \frac{\partial \theta_j}{\partial z} \end{bmatrix}. \quad (29)$$

The following lemma can be proven using the basic properties of parities.

Lemma 5.1

If $\phi_i = (u_i, v_i, \theta_i) \in \mathcal{X}^3 \cap H_1, i = 1, 2$, then for $i, j, k = 1, 2$,

1. $-s(g_1(\phi_i, \phi_j)) = s(g_2(\phi_i, \phi_j)) = s(g_3(\phi_i, \phi_j)) = (s_x(w_i w_j), -s_z(w_i w_j))$.
2. $s(g_k(\phi_i, \phi_j)) = s(g_k(\phi_j, \phi_i))$.

Hereafter, without loss of generality, we will assume that

$$\phi_1 \text{ is of parity class 1 and } \phi_2 \text{ is of parity class 2,} \quad (30)$$

which are as given in Table I.

Using Lemma 5.1, we can prove

Lemma 5.2

Under the assumption (30),

$$s(g_2(\phi_1, \phi_1)) = s(g_2(\phi_2, \phi_2)) = (1, -1), \quad s(g_2(\phi_1, \phi_2)) = (-1, -1).$$

Lemma 5.3

Under the assumption (30), $P_2G(\phi_i, \phi_j) = G(\phi_i, \phi_j)$ for $i, j = 1, 2$.

Table III. Parities of the first two critical modes and the center manifold functions.											
ψ_1	ϕ_1	θ_1	ψ_2	ϕ_2	θ_2	Ψ_1	Θ_1	Ψ_2	Θ_2	Ψ_3	Θ_3
(e, e)	(o, e)	(o, e)	(e, e)	(o, o)	(e, o)	(e, o)	(o, o)	(o, o)	(o, o)	(o, o)	(e, o)

Proof

Note that $P_2G(\phi_i, \phi_j) = G(\phi_i, \phi_j)$ if $(G(\phi_i, \phi_j), \phi_k) = 0$ for $i, j, k = 1, 2$. Now,

$$(G(\phi_i, \phi_j), \phi_k) = \int_{\Omega} (g_1(\phi_i, \phi_j)u_k + g_2(\phi_i, \phi_j)w_k + g_3(\phi_i, \phi_j)\theta_k) dx dz. \tag{31}$$

By Lemma 5.1 and Lemma 5.2, $g_1(\phi_i, \phi_j)$ is even in the z-direction while $g_2(\phi_i, \phi_j)$ and $g_3(\phi_i, \phi_j)$ are odd in the z-direction. Because u_k is odd and w_k and θ_k are even in the z-direction, the integral in (31) must vanish over Ω . \square

Thus, by Lemma 5.3 and equation (28), $\Phi_i = (U_i, W_i, \Theta_i)$, ($i = 1, 2, 3$) are solutions of

$$\begin{aligned} -\mathcal{L}_R\Phi_1 &= G(\phi_1, \phi_1), \\ -\mathcal{L}_R\Phi_2 &= G(\phi_1, \phi_2) + G(\phi_2, \phi_1), \\ -\mathcal{L}_R\Phi_3 &= G(\phi_2, \phi_2). \end{aligned} \tag{32}$$

Using the stream function $\Psi_z = U$, $\Psi_x = -W$, one can eliminate the pressure from these equations to obtain

$$\begin{aligned} \text{Pr}\Delta^2\Psi - \sqrt{R}\sqrt{\text{Pr}}\frac{\partial\Theta}{\partial x} &= h_1 := -\frac{\partial g_1}{\partial z} + \frac{\partial g_2}{\partial x}, \\ -\sqrt{R}\sqrt{\text{Pr}}\frac{\partial\Psi}{\partial x} + \Delta\theta &= h_2 := -g_3, \\ \Psi = \frac{\partial\Psi}{\partial n} &= \Theta = 0 \text{ on } \partial\Omega. \end{aligned} \tag{33}$$

Lemma 5.4

Under the assumption (30), the center manifold functions have the parity as given in Table III.

Proof

We can eliminate Θ from the first equation of (33) to obtain

$$\begin{aligned} \text{Pr}\Delta^3\Psi - R\text{Pr}\frac{\partial^2\Psi}{\partial x^2} &= \Delta h_1 + \sqrt{R}\sqrt{\text{Pr}}\frac{\partial h_2}{\partial x}, \\ \Delta\Theta &= h_2 + \sqrt{R}\sqrt{\text{Pr}}\frac{\partial\Psi}{\partial x}. \end{aligned} \tag{34}$$

Now using Lemma 5.1 and Lemma 5.2, we see that $s(\Psi) = (-s_x(g_2), s_z(g_2))$ and $s(\Theta) = s(g_2)$. \square

Using Table III, we find that the integrands in $a_{12}, a_{14}, a_{21}, a_{23}$ are all odd functions of z, and hence, we have the following.

Lemma 5.5

Under the assumption (30), in (27), we have

$$a_{12} = a_{14} = a_{21} = a_{23} = 0.$$

As a result of Lemma 5.5, we obtain the reduced equations (20).

Step 3. The attractor bifurcation. Now, we will prove that the bifurcated attractor is homeomorphic to S^1 . For this, we will need the following result.

Theorem 5.6 (Ma and Wang [15])

Let v be a 2D C^r ($r \geq 1$) vector field given by

$$v_{\lambda}(x) = \beta(\lambda)x - h(x, \lambda), \tag{35}$$

for $x \in \mathbb{R}^2$. Here, $\beta(\lambda)$ is a continuous function of λ satisfying $\beta(\lambda) \geq 0$ for $\lambda \geq \lambda_0$ and

$$h(x, \lambda) = h_k(x, \lambda) + o(|x|^k), \quad C_1|x|^{k+1} \leq (h_k(x, \lambda), x),$$

for some odd integer $k \geq 3$ where $h_k(\cdot, \lambda)$ is a k -multilinear field, and $C_1 > 0$ is some constant. Then, the system

$$dx/dt = v_{\lambda}(x), \quad x \in \mathbb{R},$$

bifurcates from $(x, \lambda) = (0, \lambda_0)$ to an attractor Σ_{λ} , which is homeomorphic to S^1 , for $\lambda_0 < \lambda < \lambda_0 + \epsilon$, for some $\epsilon > 0$. Moreover, either (i) Σ_{λ} is a periodic orbit, or (ii) Σ_{λ} consists of an infinite number of singular points, or (iii) Σ_{λ} contains at most $2(k + 1)$ singular points, consisting of $2N$ saddle points, $2N$ stable node points, and $n(\leq 2(k + 1) - 4N)$ singular points with index zero.

Now let

$$h(y_1, y_2) = \{y_1 (a_{11}y_1^2 + a_{13}y_2^2), y_2 (a_{22}y_1^2 + a_{24}y_2^2)\}^T.$$

Lemma 5.7

Assume that $\Phi_i \neq 0$ for $i = 1, 2, 3$. Then for any $y = (y_1, y_2)$,

$$(h(y), y) = a_{11}y_1^4 + (a_{13} + a_{22})y_1^2y_2^2 + a_{24}y_2^4 \leq C|y|^4, \quad (36)$$

where $C < 0$.

Proof

$$\begin{aligned} a_{11} &= G_s(\phi_1, \Phi_1, \phi_1) = G(\phi_1, \Phi_1, \phi_1) + G(\Phi_1, \phi_1, \phi_1) \\ &= G(\phi_1, \Phi_1, \phi_1) = -G(\phi_1, \phi_1, \Phi_1) = (\mathcal{L}_R \Phi_1, \Phi_1). \end{aligned} \quad (37)$$

Here, we used (32) and the following properties of the Navier–Stokes nonlinearity

$$(i) G(\phi, \tilde{\phi}, \phi^*) = G(\phi, \phi^*, \tilde{\phi}), \quad (ii) G(\phi, \tilde{\phi}, \tilde{\phi}) = 0, \quad (38)$$

and $-\mathcal{L}_R \Phi_1 = G(\phi_1, \phi_1)$, which is due to (32).

If we write

$$\Phi_j = \sum_{k=3}^{\infty} c_{j,k} \phi_k, \quad j = 1, 2, 3,$$

then for $j = 1, 2, 3$,

$$(\mathcal{L}_R \Phi_j, \Phi_j) = \sum_{k=3}^{\infty} c_{j,k}^2 \beta_k \|\phi_k\|^2 < 0. \quad (39)$$

Because $\beta_k < 0$ for $k \geq 3$ and by assumption, there exists $k \geq 3$ such that $c_{1,k} \neq 0$. In particular, $a_{11} < 0$. As in (37), we can show that

$$a_{24} = G_s(\phi_2, \Phi_3, \phi_2) = (\mathcal{L}_R \Phi_3, \Phi_3) < 0.$$

Now if $a_{13} + a_{22} < 0$, then it is easy to prove (36). Assume otherwise. Using (38) and (32), we can write

$$\begin{aligned} a_{13} &= G_s(\phi_1, \Phi_3, \phi_1) + G_s(\phi_2, \Phi_2, \phi_1) \\ &= G(\phi_1, \Phi_3, \phi_1) + G(\Phi_3, \phi_1, \phi_1) + G_s(\phi_2, \Phi_2, \phi_1) \\ &= -(G(\phi_1, \Phi_3) + G_s(\phi_2, \Phi_2, \phi_1)) \\ &= (\mathcal{L}_R \Phi_1, \Phi_3) + G_s(\phi_2, \Phi_2, \phi_1). \end{aligned} \quad (40)$$

A similar computation shows

$$a_{22} = (\mathcal{L}_R \Phi_3, \Phi_1) + G_s(\phi_1, \Phi_2, \phi_2). \quad (41)$$

Let us define

$$\alpha = G_s(\phi_1, \Phi_2, \phi_2) + G_s(\phi_2, \Phi_2, \phi_1). \quad (42)$$

By (38) and (32),

$$\alpha = -(G(\phi_1, \phi_2) + G(\phi_2, \phi_1), \Phi_2) = (\mathcal{L}_R \Phi_2, \Phi_2). \quad (43)$$

Note that $\alpha < 0$ by (39). By using Cauchy–Schwarz inequality and the orthogonality of the eigenfunctions,

$$\begin{aligned} (\mathcal{L}_R \Phi_1, \Phi_3) &= \sum_{k=3}^{\infty} \beta_k c_{1,k} c_{3,k} \|\phi_k\|^2 \\ &\leq \left(\sum_{k=3}^{\infty} -\beta_k c_{1,k}^2 \|\phi_k\|^2 \right)^{1/2} \left(\sum_{k=3}^{\infty} -\beta_k c_{3,k}^2 \|\phi_k\|^2 \right)^{1/2} \\ &= \sqrt{a_{11} a_{24}}. \end{aligned} \quad (44)$$

Because $(\mathcal{L}_R \Phi_3, \Phi_1) = (\mathcal{L}_R \Phi_1, \Phi_3)$, we have by (40)–(44),

$$a_{13} + a_{22} < 2\sqrt{a_{11} a_{24}} + \alpha,$$

where $\alpha < 0$ is given by (42). Thus, there exists $0 < \epsilon_1 < -a_{11}$, $0 < \epsilon_2 < -a_{24}$ such that

$$a_{13} + a_{22} < 2\sqrt{a_{11} a_{24}} + \alpha < 2\sqrt{(a_{11} + \epsilon_1)(a_{24} + \epsilon_2)}.$$

Because $2ab < a^2 + b^2$, we have

$$2\sqrt{(a_{11} + \epsilon_1)(a_{24} + \epsilon_2)} y_1^2 y_2^2 \leq -(a_{11} + \epsilon_1) y_1^4 - (a_{24} + \epsilon_2) y_2^4.$$

Now, let $C = \max\{-\epsilon_1, -\epsilon_2\}$. Then, $C < 0$, and we have

$$(h(y), y) \leq a_{11}y_1^4 + (a_{13} + a_{22})y_1^2y_2^2 + a_{24}y_2^4 \leq C(x^2 + y^2)^2.$$

That finishes the proof. □

Thus, by Theorem 5.6 and Lemma 5.7, Σ_R is homeomorphic to S^1 . Now we will describe the details of its structure by determining the bifurcated steady states and their stabilities.

Step 4. The steady states and their stabilities. The possible equilibrium solutions of the truncated equations of (20) are as follows.

$$R_1 = \left(\sqrt{\frac{\beta_1}{-a_{11}}}, 0 \right), R_2 = \left(0, \sqrt{\frac{\beta_2}{-a_{24}}} \right), M = \left(\sqrt{\frac{D_2}{D_3}}, \sqrt{\frac{D_1}{D_3}} \right), \quad (45)$$

where D_1, D_2 , and D_3 are given by (21).

Because of the invariance of the equations (20) with respect to $(x, y) \rightarrow (-x, y)$ and $(x, y) \rightarrow (x, -y)$, we only consider the positive solutions when writing (45).

The eigenvalues λ_1, λ_2 of the truncated vector field at the steady states R_1, R_2 are

$$\lambda_1^{R_1} = -2\beta_1, \lambda_2^{R_1} = -D_1/a_{11}, \lambda_1^{R_2} = -2\beta_2, \lambda_2^{R_2} = -D_2/a_{24}.$$

Note that R_i is always bifurcated for $\beta_i > 0, i = 1, 2$. Moreover, R_i is a stable steady state for $\beta_i > 0$ if $D_i < 0$ for $i = 1, 2$. The trace Tr and the determinant Det of the Jacobian matrix of the truncated vector field at the mixed states M are

$$Tr = \frac{2}{D_3}(a_{24}D_1 + a_{11}D_2), \quad Det = \frac{4}{D_3}D_1D_2. \quad (46)$$

Notice that the steady states M are bifurcated only when D_1, D_2, D_3 have the same sign. Because a_{11} and a_{24} are both negative as shown in Lemma 5.7, according to trace-determinant plane analysis, they are saddles if $D_1 < 0, D_2 < 0, D_3 < 0$ and are stable if $D_1 > 0, D_2 > 0, D_3 > 0$.

Finally, only the four cases stated in our main theorem can occur. To see this, note that according to Theorem 5.6 and (45)–(46), the case $D_1 < 0, D_2 < 0, D_3 > 0$ is not possible because that would lead to only four steady states on the attractor, which are all stable. Similarly, the case $D_1 > 0, D_2 > 0, D_3 < 0$ is not possible either, which would lead to four steady states, which are all unstable.

6. Numerical approximation of the coefficients of the reduced equations

To compute the coefficients of the reduced equations (20), we fix L, Pr , and R to compute all the eigenvalues β_i^N and the corresponding eigenvectors of (16).

Numerical computation of the center manifold functions. Now we will numerically approximate Φ_1, Φ_2 , and Φ_3 , which are the solutions of the equations (28). We will illustrate the method to approximate Φ_1 because Φ_2, Φ_3 can be approximated similarly. To determine Φ_1 , we have to find its stream function Ψ and its temperature function Θ , which are determined by the equations (33).

Because we do not have h_1 and h_2 in (33) exactly, we approximate them by h_1^N, h_2^N as that shown later.

$$\begin{aligned} h_1^N &= -\frac{\partial g_1^N}{\partial z} + \frac{\partial g_2^N}{\partial x}, & h_2^N &= \psi_{1,z}^N \theta_{1,x}^N - \psi_{1,x}^N \theta_{1,z}^N, \\ g_1^N &= -\psi_{1,z}^N \psi_{1,xz}^N + \psi_{1,x}^N \psi_{1,zz}^N, & g_2^N &= -\psi_{1,z}^N \psi_{1,xx}^N + \psi_{1,x}^N \psi_{1,xz}^N. \end{aligned} \quad (47)$$

Here, (ψ_1^N, θ_1^N) is the first critical eigenfunction of the discrete problem (16).

$$\{\psi_1^N, \theta_1^N\} = \sum_{m=0}^{N_x-1} \sum_{n=0}^{N_z-1} \left\{ \tilde{\psi}_{1,mn}^N e_m(x) e_n(z), \tilde{\theta}_{1,mn}^N f_m(x) f_n(z) \right\}. \quad (48)$$

The Legendre–Galerkin approximation of the problem (33). As in the linear eigenvalue problem, we discretize the equations (33) using the generalized Jacobi polynomials (11)–(12).

$$\{\Psi^N, \Theta^N\} = \sum_{m=0}^{N_x-1} \sum_{n=0}^{N_z-1} \left\{ \tilde{\Psi}_{mn}^N e_m(x) e_n(z), \tilde{\Theta}_{mn}^N f_m(x) f_n(z) \right\}. \quad (49)$$

We plug in $\Psi^N, \Theta^N, h_1^N, h_2^N$ for Ψ, Θ, h_1, h_2 in (33) and multiply the resulting equations by Jacobi polynomials $e_j(x)e_k(z), f_j(x)f_k(z)$ and integrate over $-1 \leq x \leq 1, -1 \leq z \leq 1$ to reduce (33) to the following finite dimensional linear equation

$$(B^N - \sqrt{R}C^N) \bar{x} = \bar{b}. \quad (50)$$

Here, B^N and C^N are given by (17) and

$$\bar{x} = [\text{vec}(\tilde{\Psi}^N) \text{vec}(\tilde{\Theta}^N)]_{N^2 \times 1}^T, \quad \bar{b} = [\text{vec}(B_1) \text{vec}(B_2)]^T. \tag{51}$$

For $0 \leq j \leq N_x - 1, 0 \leq k \leq N_z - 1,$

$$(B_1)_{jk} = \int_{-1}^1 \int_{-1}^1 h_1^N(x, z) e_j(x) e_k(z) dx dz, \tag{52}$$

$$(B_2)_{jk} = \int_{-1}^1 \int_{-1}^1 h_2^N(x, z) f_j(x) f_k(z) dx dz.$$

Now, e_j is a polynomial of degree $j + 4$, and by (47) and (48), h_1^N is a polynomial of degree at most $(2N_x + 6, 2N_z + 6)$. Thus, the aforementioned integrands are of degree at most $(3N_x + 9, 3N_z + 9)$. Because the Legendre–Gauss–Lobatto quadrature with $N + 1$ quadrature points is exact for polynomials of degree less or equal than $2N - 1$, the integrals in (52) can be replaced by the following discrete inner products.

$$(B_1)_{jk} = \sum_{m=0}^{\frac{3}{2}N_x+5} \sum_{n=0}^{\frac{3}{2}N_z+5} h_1^N(x_m, z_n) e_j(x_m) e_k(z_n) \omega_m^x \omega_n^z, \tag{53}$$

$$(B_2)_{jk} = \sum_{m=0}^{\frac{3}{2}N_x+5} \sum_{n=0}^{\frac{3}{2}N_z+5} h_2^N(x_m, z_n) f_j(x_m) f_k(z_n) \omega_m^x \omega_n^z.$$

Here, $\{x_j, w_j^x\}_{j=0}^{\frac{3}{2}N_x+5}$ and $\{z_j, w_j^z\}_{j=0}^{\frac{3}{2}N_z+5}$ are the Legendre–Gauss–Lobatto points and weights in the x -direction and the z -direction.

Solution of (50). The solution \bar{x} of (50) can be obtained by inverting the matrix $(B^N - \sqrt{R} C^N)$. But this matrix has a large condition number. Thus, we show a method to obtain the solution inverting the matrix D^N given by (17), which has a much smaller condition number. For example, for $N_x = 10, N_z = 8$, the condition number of $(B^N - \sqrt{R} C^N)$ is $O(10^{16})$ while the condition number of D^N is $O(10^8)$.

Because $\Phi_1 \in E_2 = \text{span}\{\phi_1, \phi_2\}^\perp$, we look for a solution of (50) in the form

$$\bar{x} = \sum_{i=3}^N x_i \bar{x}_i, \tag{54}$$

where \bar{x}_i are the eigenvectors of

$$B^N \bar{x}_i - \sqrt{R} C^N \bar{x}_i = \beta_i(R) D^N \bar{x}_i. \tag{55}$$

If we multiply (50) by $(D^N)^{-1}$ and use (55), the left-hand side of (50) becomes

$$\sum_{i=3}^N x_i \beta_i(R) \bar{x}_i = (D^N)^{-1} (B^N - \sqrt{R} C^N) \bar{x} = (D^N)^{-1} \bar{b} := \bar{f}. \tag{56}$$

We determine \bar{f} from $D^N \bar{f} = \bar{b}$ using Gaussian elimination. Once again using Gaussian elimination, we can find the coefficients f_i in the expansion

$$\bar{f} = \sum_{i=1}^N f_i \bar{x}_i. \tag{57}$$

In (57), we see that $f_1 = f_2 = 0$ is necessary for the existence of a solution of (50). From (56) and (57), one finds $x_i = f_i / \beta_i(R)$, $i = 3, 4, \dots, N$. Thus, the Jacobi expansion coefficients in (49) of the center manifold are given by

$$\text{vec}(\tilde{\Psi}^N) = \sum_{i=3}^N \frac{f_i}{\beta_i(R)} \text{vec}(\tilde{\psi}_i^N), \quad \text{vec}(\tilde{\Theta}^N) = \sum_{i=3}^N \frac{f_i}{\beta_i(R)} \text{vec}(\tilde{\theta}_i^N).$$

Numerical computation of a_{ij} in (27). We approximate a_{11} by

$$a_{11}^N = G_s(\phi_1^N, \Phi_1^N, \phi_1^N). \tag{58}$$

The integrands in $G_s(\phi_1^N, \Phi_1^N, \phi_1^N)$ are polynomials of degree at most $(3N_x + 9, 3N_z + 9)$. Thus, to replace the integrals in (58), one needs again $(\frac{3}{2}N_x + 5, \frac{3}{2}N_z + 5)$ quadrature points and nodes in the numerical inner product. The other coefficients a_{ij} in (27) are approximated similarly.

Table IV. The coefficients of the reduced equations for various Pr values at the first three critical length scales.

Pr	$L_c = 1.5702$		$L_c = 2.6611$		$L_c = 3.7048$	
	$a_{22} \times 10^2$	$D_3 \times 10^5$	$a_{22} \times 10^2$	$D_3 \times 10^5$	$a_{22} \times 10^2$	$D_3 \times 10^5$
0.01	7.6492	2559.8276	-23.7252	140.2894	-20.5185	-15.6696
0.04	0.1313	93.3662	-6.0784	3.6690	-5.3093	-1.4416
0.05	-0.4546	50.5609	-5.0374	1.0455	-4.4332	-1.1525
0.06	-0.8740	29.9252	-4.3902	-0.2713	-3.8966	-1.0122
0.14	-2.3697	0.6458	-3.0486	-2.3788	-2.8749	-0.9899
0.15	-2.4662	-0.0707	-3.0218	-2.4414	-2.8641	-1.0182
0.71	-3.2469	-9.5827	-2.8940	-2.5437	-2.8848	-1.4316
7	-0.8551	-0.8348	-0.7484	-0.1610	-0.7444	-0.0987
100	-0.0687	-0.0055	-0.0599	-0.0010	-0.0595	-0.0006
1000	-0.0069	-0.0001	-0.0060	-0.00001	-0.0060	-0.000006

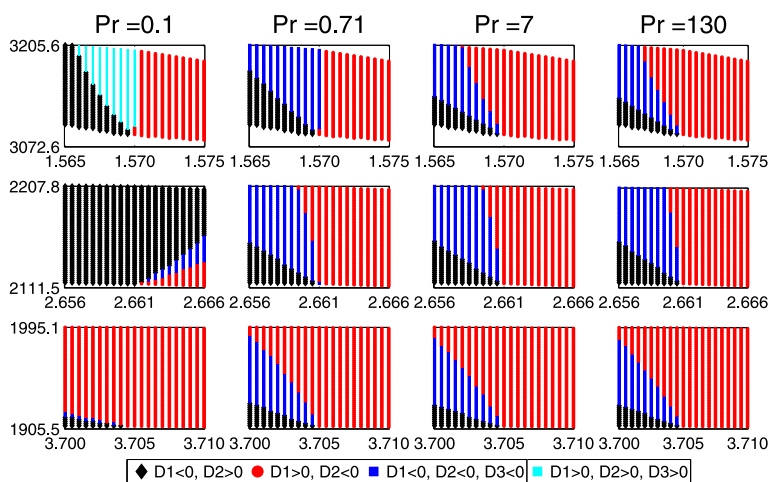


Figure 6. The signs of D_1 , D_2 , and D_3 in the L - R plane. In each subfigure, the x and y axes denote the length scale L and the Rayleigh number R , respectively. For each column, the Prandtl number is given earlier.

Remark 6.1

We observed that increasing N_x and N_z above $N_x = 10 + 2k$ and $N_z = 8$ only changes a_{ij}^N in the seventh digit when the first critical mode has k rolls and the second critical mode has $k + 1$ rolls in their stream functions.

7. Numerical results and discussion

We computed coefficients of the reduced equations for various Pr values ranging from 0.1 to 10^3 at the first three critical length scales and at the critical Rayleigh numbers, which are given in Table II.

As proven in Theorem 4.1, the coefficients a_{11} and a_{24} are always negative. In our numerical calculations, we encountered that a_{13} is also always negative. But the sign of a_{22} and the sign of D_3 depend on L and Pr and are given in Table IV.

For the first critical length scale $L_c = 1.5702$, we found that a_{22} and D_3 change sign from positive to negative between $0.04 < Pr < 0.05$ and $0.14 < Pr < 0.15$, respectively. Thus, the transition is as described in Figure 5(a) for $Pr < 0.04$, as in Figure 5(b) for $0.05 < Pr < 0.14$, and as in Figure 5(c) for $Pr > 0.15$. Thus, the mixed modes can be stable when $Pr < 0.14$, but only the pure modes are stable points of the attractor when $Pr > 0.15$.

For the second critical length scale $L_c = 2.6611$, we always observed that $a_{22} < 0$. However, D_3 changes sign between $0.05 < Pr < 0.06$. Thus, the transition is as described in Figure 5(b) for $Pr < 0.05$ and as described in Figure 5(c) for $Pr > 0.06$. In particular, the mixed modes can be stable when $Pr < 0.05$, but only the pure modes are stable steady states when $Pr > 0.06$.

For higher critical length scales (third and beyond), we found that $a_{22} < 0$ and $D_3 < 0$ for the Prandtl numbers we considered. Thus, the transition is as described in Figure 5(c). For this length scale, either the critical Prandtl number that was observed for the first two critical length scales is now very close to zero, or it does not exist at all.

The previous analysis depends on the coefficients a_{ij} of the reduced equations and predicts the transitions when both eigenvalues β_1, β_2 are close to zero. Now, we present an analysis depending on the direct computation of the numbers D_1, D_2 (both of which vanish when $\beta_1 = \beta_2 = 0$), and D_3 . We computed D_1, D_2 , and D_3 for L and R values around (but not necessarily very close to) the criticality $(L, R) = (L_c, R_c)$ for the first three critical length scales and for Prandtl numbers $Pr = 0.1, 0.71, 7, 130$. The results are shown in Figure 6.

Although we might have omitted the smallness assumptions of $|L - L_c|$ and $|R - R_c|$ where our main theorem is valid, these figures help us predict the transitions in the L - R plane. The results we obtain are as follows.

For $Pr = 0.71$, $Pr = 7$, $Pr = 130$, transitions are qualitatively the same in the L - R plane. For $L > L_c$, the basic motionless state loses its stability to the eigenmode with wave number $k + 1$ as the Rayleigh number crosses the first critical Rayleigh number and further increase of the Rayleigh number does not alter the stability of this steady state. This is in contrast to the situation $L < L_c$ where there is a transition of stabilities as the Rayleigh number is increased. Namely, as the Rayleigh number crosses the first critical Rayleigh number, the eigenmode with wave number k becomes stable. As the Rayleigh number is further increased, both eigenmodes coexist as stable steady states and the initial conditions determine which one of these steady states will be realized. Finally, as the Rayleigh number is further increased, the eigenmode with wave number $k + 1$ becomes stable.

The transition at $Pr = 0.1$ is essentially different than for those at $Pr = 0.71, 7, 130$. In particular, for the first critical length scale $L_c = 1.5702$, for $L < L_c$, subsequently, mode with wave number k , mixed modes, and finally mode with wave number $k + 1$ will be realized as the Rayleigh number is increased while for $L > L_c$, $k + 1$ mode is the only stable steady state.

Acknowledgements

The work of Shen is partially supported by NSF-DMS-1217066 and DMS-1419053, and the work of Wang is supported in part by NSF-DMS-1211218.

References

1. Davies-Jones RP. Thermal convection in an infinite channel with no-slip sidewalls. *Journal of Fluid Mechanics* 1970; **44**(4):695–704.
2. Luijckx JM, Platten JK. On the onset of free convection in a rectangular channel. *Journal of Non-Equilibrium Thermodynamics* 1981; **6**(3):141–158.
3. Kato Y, Fujimura K. Prediction of pattern selection due to an interaction between longitudinal rolls and transverse modes in a flow through a rectangular channel heated from below. *Physical Review E* 2000; **62**(1):601–611.
4. Lee NY, Schultz WW, Boyd JP. Stability of fluid in a rectangular enclosure by spectral method. *International Journal of Heat and Mass Transfer* 1989; **32**(3):513–520.
5. Mizushima J. Onset of the thermal convection in a finite two-dimensional box. *Journal of the Physical Society of Japan* 1995; **64**(7):2420–2432.
6. Gelfgat AY. Different modes of Rayleigh–Bénard instability in two- and three-dimensional rectangular enclosures. *Journal of Computational Physics* 1999; **156**(2):300–324.
7. Ma T, Wang S. Dynamic bifurcation and stability in the Rayleigh–Bénard convection. *Communications in Mathematical Sciences* 2004; **2**:159–183.
8. Ma T, Wang S. Rayleigh–Bénard convection: dynamics and structure in the physical space. *Communications in Mathematical Sciences* 2007; **5**(3):553–574.
9. Sengul T, Wang S. Pattern formation in Rayleigh–Bénard convection. *Communications in Mathematical Sciences* 11 2013; **1**:315–343.
10. Orszag SA. Accurate solution of the Orr–Sommerfeld stability equation. *Journal of Fluid Mechanics* 1971; **50**(4):689–703.
11. Hill AA, Straughan B. A Legendre spectral element method for eigenvalues in hydrodynamic stability. *Journal of computational and applied mathematics* 2006; **193**(1):363–381.
12. Gheorghiu CI, Dragomirescu FI. Spectral methods in linear stability. Applications to thermal convection with variable gravity field. *Applied Numerical Mathematics* 2009; **59**(6):1290–1302.
13. Ma T, Wang S. *Phase Transition Dynamics*. Springer-Verlag, 2013.
14. Foias C, Manley O, Teman R. Attractors for the Bénard problem: existence and physical bounds on their fractal dimension. *Nonlinear Analysis* 1987; **11**(8):939–967.
15. Ma T, Wang S. *Bifurcation Theory and Applications*, Vol. 53. World Scientific Publishing: Singapore, 2005.
16. Hydon PE. *Symmetry Methods for Differential Equations: A Beginner's Guide*, Vol. 22. Cambridge University Press: Cambridge, UK, 2000.
17. Marques F, Lopez JM, Blackburn HM. Bifurcations in systems with Z_2 spatio-temporal and $O(2)$ spatial symmetry. *Physica D: Nonlinear Phenomena* 2004; **189**(3):247–276.
18. Shen J. Efficient spectral-Galerkin method I. Direct solvers of second- and fourth-order equations using Legendre polynomials. *SIAM Journal on Scientific Computing* 1994; **15**(6):1489–1505.
19. Shen J, Tang T, Wang L. *Spectral Methods: Algorithms, Analysis and Applications*, Vol. 40. Springer Verlag, 2011.
20. Guo B, Shen J, Wang L. Optimal spectral-Galerkin methods using generalized Jacobi polynomials. *Journal of Scientific Computing* 2006; **27**(1–3):305–322.
21. Mizushima J, Nakamura T. Repulsion of eigenvalues in the Rayleigh–Bénard problem. *Journal of the Physical Society of Japan* 2002; **71**:677.